

N-Type Oxide Thermoelectrics Via Visual Search Strategies

Guangzong Xing¹, Jifeng Sun², Khuong P. Ong³, Xiaofeng Fan¹, Weitao Zheng¹, and David J. Singh²

¹*College of Materials Science and Engineering,
Jilin University, 130012, Changchun, China*

²*Department of Physics and Astronomy,
University of Missouri, Columbia,
Missouri, 65211-7010, USA*

³*Institute of High Performance Computing,
Agency for Science Technology and Research,*

1 Fusionopolis Way, 16-16 Conneris, 138632 Singapore

(Dated: September 11, 2018)

We discuss and present search strategies for finding new thermoelectric compositions based on first principles electronic structure and transport calculations. We illustrate them by application to a search for potential n-type oxide thermoelectric materials. This includes a screen based on visualization of electronic energy isosurfaces. We report compounds that show potential as thermoelectric materials along with detailed properties, including SrTiO₃, which is a known thermoelectric, and appropriately doped KNbO₃ and rutile TiO₂.

Thermoelectrics are an energy conversion technology that is used in spacecraft power generation, portable coolers and other areas. [1–4] The direct thermal to electrical energy conversion provided by this technology and its scalability to low size and power suggests numerous potential applications. [5, 6] However, this is limited by the low efficiency of existing devices, in turn limited by the performance of known thermoelectric materials. The maximum efficiency is governed by a dimensionless, but temperature dependent figure of merit, $ZT = \sigma S^2 T / \kappa$, where T is absolute temperature, σ is electrical conductivity, S is thermopower (also known as the Seebeck coefficient) and κ is the thermal conductivity, usually written as a sum of electronic and lattice contributions, $\kappa = \kappa_e + \kappa_l$, which is typically a good approximation.

Thermoelectric materials pose a particular challenge to materials genome approaches. This is because thermoelectric performance, characterized by a figure of merit, ZT , is a contraindicated property of matter. In particular, standard common models, such as the isotropic parabolic band model, with normal assumptions predict that high ZT will not occur. This means that very high performance thermoelectric materials have unusual electronic features, a number of which have been proposed and identified as important in various cases. These include reduced dimensionality, either in artificial structures [7] or due to details of band formation, and other complex electronic structure characteristics. [8–18]

Most good thermoelectric materials, such as (Bi,Sb)₃Te₂, PbTe, Si-Ge, skutterudites and Mg₂(Si,Sn) are narrow to moderate gap semiconductors. Several papers reporting searches for new semiconductors with thermoelectric potential have been reported. [19–22] However, there are several thermoelectric materials that do not fit in the category of moderate band gap semiconductors, including some oxides. Oxides can potentially offer a number of advantages for application

including perhaps low cost ceramic materials processing. [23, 24] The high ZT oxide thermoelectrics are Na_xCoO₂ and closely related p-type layered Co and Rh oxides, with figures of merit approaching $ZT \sim 1$. [25–28] The best n-type oxide thermoelectrics are very different, and the best n-type ZT values barely exceed 0.5. This is found in ZnO ceramics at very high temperature. [29–31] This is an oxide semiconductor with a substantial gap.

A particular challenge in finding new oxide thermoelectrics is that ZT depends strongly on doping level, among other material parameters, and therefore assessing the potential of a given material requires detailed doping studies. Here we demonstrate some simple measures that can be readily calculated from first principles and used in searching for new oxide thermoelectrics. For this purpose, we use a set of early transition metal and simple oxides, selected with a view to having oxides that are at least potentially dopable n-type, based on the criterion that they either are known to be dopable or that they have the same transition element and similar coordination to a dopable material. The list includes two known transparent conductors, In₂O₃ and BaSnO₃, several niobates and titanates as well as BaZrO₃ for comparison. We focus on high temperature because the thermoelectric performance generally increases with temperature for wide band gap materials, and so if there are any high ZT n-type oxide thermoelectrics in this class, they are likely to have their best performance at high temperatures. We note that several of these materials have complex heavy valence band structures, which might suggest p-type thermoelectricity. However, these compounds are all naturally n-type, and p-type doping is unlikely to be feasible; we do not pursue this further.

The calculations were performed consistently for all compounds. The first principles calculations used the general potential linearized augmented planewave (LAPW) method, [32] as implemented in the WIEN2k code, [33] with well converged LAPW basis sets, includ-

ing local orbitals for semicore states. Experimental lattice parameters were used, while atomic coordinates were determined by energy minimization, subject to the experimental space group symmetry. This was done with the generalized gradient approximation functional of Perdew, Burke and Ernzerhof (PBE-GGA). [34] Electronic structures were then calculated using the modified Becke-Johnson potential of Tran and Blaha (mBJ), [35] which improves band gaps of these materials relative to PBE. [35–39] Transport coefficients were obtained from the electronic structures using the constant scattering time approximation and the BoltzTraP code. [40] The Seebeck coefficients presented are all ceramic averages, defined by $S_{av} = (\sigma_{xx}S_{xx} + \sigma_{yy}S_{yy} + \sigma_{zz}S_{zz})/(\sigma_{xx} + \sigma_{yy} + \sigma_{zz})$, where σ is the electrical conductivity.

In order to develop screens for thermoelectric oxides, it is useful to begin with a parabolic band model. For a degenerate doped single parabolic band (SPB), effective mass, m^* , the Seebeck coefficient at low temperature ($k_B T \ll E_F$) in the constant scattering time approximation is given by

$$S = \frac{8\pi^2 k_B^2 m^* T}{3e\hbar^2} \left(\frac{\pi}{3n}\right)^{2/3} = \frac{\pi^2 k_B}{2e} \frac{k_B T}{E_F}, \quad (1)$$

where E_F is measured from the band edge (note e is negative). Thus $S(T)$ increases linearly with effective mass and temperature, and decreases as the 2/3 power of carrier concentration. The expression in terms of E_F holds more generally for a degenerate doped single parabolic band, regardless of the anisotropy of the effective mass tensor and importantly, when written in terms of the energy, S is independent of m^* . [41, 42] The volumetric density of states is $N(E) = (V/2\pi^2)(2m/\hbar^2)^{3/2}E_F^{1/2}$.

The conductivity for a doped SPB under the same conditions is given by $\sigma = ne^2\tau/m^*$, where τ is an effective inverse scattering rate. For an anisotropic parabolic band $1/m^*$ is replaced by an inverse effective mass tensor and the conductivity tensor takes the anisotropy of this tensor. Thus σS^2 , which is in the numerator of ZT varies as $m^*\tau/n^{1/3}$. τ generally decreases with both m^* and n . Thus this formula does not mean that high effective mass by itself is sufficient to get high ZT .

These formulas imply that if one considers different semiconducting compounds one should expect a wide range of doping dependent thermopowers. This is seen in the left panel of Fig. 1, which shows the doping dependent $S(1000\text{ K})$ for the compounds investigated here. On the other hand, the various compounds appear more similar at fixed energy. This is seen in the right panel of the figure, which shows the $S(1000\text{ K})$ as a function of Fermi energy, E_F relative to the conduction band minimum, and also in Table I. The thermopower at fixed Fermi level and temperature is relatively constant between the different phases, and in particular there is no correlation with the density of states, $N(E_F)$. The outlier compounds in right panel of Fig. 1 are $\text{Na}_2\text{Ti}_3\text{O}_7$ and ZnNb_2O_6 , for low S and orthorhombic NaNbO_3 for

TABLE I. Properties of the oxides investigated, including calculated band gap, E_g in eV, and electronic properties 0.1 eV above the CBM. These are the density of states, N in eV^{-1} on a per atom basis, ceramic average Seebeck at 1000 K, in $\mu\text{V}/\text{K}$, direction averaged σ/τ in $10^{18}\ \Omega\text{m}/\text{s}$, carrier concentration, n in $10^{19}\ \text{cm}^{-3}$ and conductivity anisotropy, $a = \sigma_{max}/\sigma_{min}$.

	E_g	N	S	σ/τ	n	a
BaSnO_3 $Pm\bar{3}m$	2.8	0.0039	-179	3.7	3.8	1
BaZrO_3 $Pm\bar{3}m$	4.3	0.076	-182	28.4	71.6	1
In_2O_3 $Ia\bar{3}$	3.2	0.0047	-178	4.0	4.8	1
$\text{KNbO}_3\text{-c}$ $Pm\bar{3}m$	2.4	0.147	-159	51.4	113	1
$\text{KNbO}_3\text{-r}$ $R3m$	2.8	0.121	-181	38.8	128	1.09
$\text{NaNbO}_3\text{-o}$ $Pmc2_1$	2.4	0.013	-235	12.0	37.8	1.61
$\text{NaNbO}_3\text{-r}$ $R3c$	3.4	0.160	-174	40.3	203	1.34
ZnNb_2O_6 $Pbcn$	4.1	2.23	-85	10.4	1344	3.67
CaTiO_3 $Pnma$	3.2	0.146	-183	34.6	170	1.11
$\text{Na}_2\text{Ti}_3\text{O}_7$ $P2_1/m$	4.0	0.304	-108	11.2	532	979
$\text{PbTiO}_3\text{-c}$ $Pm\bar{3}m$	2.0	0.262	-138	62.4	261	1
$\text{PbTiO}_3\text{-t}$ $P4mm$	2.1	0.102	-137	20.6	102	299
$\text{SrTiO}_3\text{-c}$ $Pm\bar{3}m$	2.7	0.158	-164	45.8	166	1
TiO_2 (ana.) $I4_1/amd$	2.9	0.034	-174	11.0	46.7	10.7
TiO_2 (rut.) $P4_2/mnm$	2.5	0.191	-175	56.7	344	1.01
$\text{Y}_2\text{Ti}_2\text{O}_7$ $Fd\bar{3}m$	3.6	0.102	-161	19.2	419	1

high S . Orthorhombic NaNbO_3 is the polar phase that exists at room temperature but becomes cubic, similar to KNbO_3 at high temperature. [43, 44] The electronic structures of cubic NaNbO_3 and cubic KNbO_3 are very similar.

The effective mass plays different roles in S and σ/τ , as is evident from the different effects of anisotropy in m^* on these two quantities. Also, as mentioned, most good thermoelectrics have band structures that differ markedly from the single isotropic parabolic band. A computational screen for potential thermoelectrics may then begin by looking for band structures that deviate from the isotropic SPB in ways that favor thermoelectric performance. To understand what kinds of band structures these are, we write the Boltzmann transport formulas for the conductivity and thermopower starting with the transport function,

$$\sigma_{\alpha\beta}(E) = e^2 \int d^3\mathbf{k} v_\alpha(\mathbf{k})v_\beta(\mathbf{k})\tau(\mathbf{k})\delta(E - E(\mathbf{k})), \quad (2)$$

where summation over bands is implied, $E(\mathbf{k})$ is the band energy and $v = \hbar^{-1}\nabla_{\mathbf{k}}E$ is the band velocity. Then the conductivity and Seebeck tensors are

$$\sigma(T) = - \int \sigma(E)f'(T, E - E_F)dE \quad (3)$$

and

$$\mathbf{S}(T) = \frac{-\sigma^{-1}(T)}{eT} \int \sigma(E)(E - E_F)f'(T, E - E_F)dE \quad (4)$$

where f' is its energy derivative of the Fermi function at temperature T .

Thus σ and S involve different integrals over the electronic structure. There are two important aspects that we use here: (1) At low temperature, Eqns. 3 and 4 have different integrals over the Fermi surface, i.e. the energy isosurface for $E = E_F$. The integrals are such that regions of high v_α^2 are highly weighted in $\sigma_{\alpha\alpha}$. For a closed isosurface these are the parts where the span across the surface is small. From this point of view, low dimensional and complex shapes are much superior to simple shapes, such as the spherical isosurface of the isotropic SPB. For example, a cylindrical isosurface is much more favorable than a sphere enclosing the same volume (number of carriers) for conduction across the cylinder. As discussed for PbTe and related thermoelectrics, [9, 13] isosurfaces with cylindrical sections in different directions can yield isotropic properties that are far superior to those that would be obtained in an SPB with the same carrier concentration. More generally, complex, corrugated isosurface shapes lead to better thermoelectric performance than the spheres that occur with an SPB. [8–10, 13–15, 17, 18] (2) At finite T , the factor $E - E_F$ makes S sensitive to the electronic structure over a wider energy range than σ . As a result, features in the electronic structure such as the onset of a heavy band near E_F can enhance S while affecting σ to a lesser extent. Examples of thermoelectrics with a light band extremum followed by onset of heavy band(s) include p-type filled skutterudites [45] and n-type lanthanum telluride. [46] Polar orthorhombic NaNbO_3 is an example of such a case, and this is the reason why it is the outlier with high S in Fig. 1. Its band structure and density of states (DOS) in comparison with some other niobates is shown in Fig. 2. The structure of the DOS is similar to p-type PbTe, [47] in contrast to the sharp onsets characteristic of the low dimensional electronic features of the cubic and rhombohedral perovskite niobates (see below). Unfortunately, as mentioned, NaNbO_3 is not in the orthorhombic polar phase at high temperature, and the particular characteristic of a heavy band onset above a light mass CBM is a result of the polar distortion. As such, while it is an interesting illustration of this effect, we do not discuss this compound further.

Most high ZT thermoelectrics have $S \sim 200 - 300 \mu\text{V/K}$ at the temperatures where they are used. This is readily understood if one applies the Wiedemann-Franz relation to the electronic part of the the thermal conductivity to obtain $ZT = \sigma S^2 T / (\kappa_l + \kappa_e) = r S^2 / L$, where $r = \kappa_e / (\kappa_l + \kappa_e) \leq 1$ and L is the Lorentz number. The standard value of L yields $ZT=1$ for $r=1$ and $S=157 \mu\text{V/K}$, or for a typical $r \sim 0.5$ with $S \sim 220 \mu\text{V/K}$. Considering the results shown in Fig. 1, this suggests a rough estimate of $E_F \sim 0.1 \text{ eV}$ for 1000 K. Isosurfaces 0.1 eV above the conduction band minimum (CBM) are shown in Fig. 3. Examination of these isosurfaces provides a very simple and fast screen since they are based on the band structure alone. For example, ZnNb_2O_6 shows

a large complex isosurface. This is characteristic of a metal, and this is why S at fixed E_F is low. Moreover, having a large complex Fermi surface at $E_F=0.1 \text{ eV}$ means that the conduction bands are extremely flat in this compound, as is also evident from the high $N(E_F)$. $\text{Na}_2\text{Ti}_3\text{O}_7$ shows a near one dimensional metallic structure, while the cylinder for tetragonal PbTiO_3 is a two dimensional electronic feature. These materials will therefore be highly anisotropic, which is not favorable for making a ceramic thermoelectric. Anatase TiO_2 has an elongated ellipsoidal shape, which again leads to large conductivity anisotropy. The transparent conductors, In_2O_3 and BaSnO_3 have small simple isosurfaces, which according to the arguments above are unfavorable, and this is also the case for pyrochlore $\text{Y}_2\text{Ti}_2\text{O}_7$.

The remaining materials have complex isosurfaces anticipated to be favorable for thermoelectric performance. The d^0 cubic perovskites and some distorted perovskites, i.e. rhombohedral KNbO_3 and NaNbO_3 and $Pnma$ CaTiO_3 , have these complex shapes because of the degeneracy of the t_{2g} orbitals in an octahedral crystal field, as was discussed previously for SrTiO_3 and KTaO_3 . [11, 12, 48] Of the compounds investigated here, cubic KNbO_3 , which is the high temperature phase, shows the most perfect low dimensional character in its band structure. This is seen in isosurfaces consisting of intersecting nearly perfect cylinders for the lowest conduction band (note that the isosurfaces are a large section consisting of three cylinders joined at the center around Γ and two small sections inside formed by the crossings of the three cylinders; in general cubic d^0 perovskites have a large jack shaped section, as seen in SrTiO_3 with two small section inside the center of the jack). Interestingly, rutile TiO_2 also shows a low dimensional character, favorable for thermoelectric performance, with isosurfaces consisting of two intersecting cylinders (note that two intersecting two dimensional, cylindrical sheets, mean that the conductivity will be three dimensional, and in TiO_2 the calculated conductivity anisotropy is weak, as shown in Table I).

The top panels of Fig. 4 show transport properties for the compounds identified based on the above screen. Additionally, in the case of KNbO_3 , which contains the $4d$ element Nb, we show results of calculations including spin-orbit. As seen, these are very similar to the scalar relativistic results. The doping range of interest for developing these materials as thermoelectrics at 1000 K ranges from $\sim 10^{20} \text{ cm}^{-3}$ for BaZrO_3 and cubic KNbO_3 to $\sim 2 \times 10^{21}$ for TiO_2 . This will shift to lower values for optimization at lower T , but as mentioned for these wide gap materials the best performance is likely to be close to the highest temperature at which the material can be used. The transport function T_1 plotted in the top right panel is $(\sigma/\tau)S^2/N^{2/3}$, where N is the volumetric density of states. The rationale for using this particular function is that it is readily computed from the band structure, that the $2/3$ power of the DOS cancels the mass dependence in the numerator for a SPB, and that

while scattering depends strongly on the details of a material, the $2/3$ power law dependence of the scattering rate on N is a reasonable choice for a degenerate doped semiconductor at high temperature. This is clearly a crude measure of the potential electronic behavior of a thermoelectric, since it makes no attempt to incorporate detailed material specific scattering mechanisms. However, it does suggest that KNbO_3 may be the best of the materials studied if it can be doped. Also, interestingly, the non-perovskite, rutile TiO_2 is within a factor of two of this “best” material. Anatase on the other hand is not favorable. The bottom left panel shows the DOS for rutile and anatase as compared with SrTiO_3 . As seen, SrTiO_3 and rutile have a similar sharp 2D-like onset at the CBM, while anatase has a lower, more 3D shape (for a 2D band, $N(E)$ has a step function shape, while for a 3D parabolic band $N(E) \propto E^{1/2}$). Bayerl and Kioupakis have reported theoretical investigation by a somewhat different approach of different TiO_2 polymorphs as potential n-type thermoelectrics and also find that rutile is exceptional. [49] The band structure of TiO_2 (bottom, right) has a double degenerate bottom conduction band at M , with a very flat CBM along the Γ - M directions. This underlies the favorable behavior.

From an experimental point of view, SrTiO_3 is known to be dopable using Nb, and $ZT \sim 0.37$ has been reported at 1000 K with 20% Nb, [50, 51] This corresponds to a very high carrier concentration, $\sim 3 \times 10^{21}$, assuming one electron per Nb. The bands at the CBM are Ti d bands, specifically from the t_{2g} level, which suggests exploration of alternate doping strategies involving the O or Sr sites. SrTiO_3 , like other perovskites near ferroelectricity, has a low thermal conductivity, which is favorable for a thermoelectric. [50–52] The thermal conductivity of NaNbO_3 is particularly low at ~ 1 W/mK at 300 K, while KNbO_3 has $\kappa \sim 10$ W/mK at this temperature. [52] Meanwhile the thermal conductivity of single crystal TiO_2 at 300 K is ~ 8 W/mK and falls with temperature to below 5 W/mK at 1000 K. [53] Furthermore it is known that TiO_2 can be doped n-type by Nb similar to SrTiO_3 . [53]

BaZrO_3 is an insulating material, with a higher band gap than SrTiO_3 and it is not known whether it can be effectively doped. Cubic PbTiO_3 has a ferroelectric transition to the tetragonal form at ~ 800 K, accompanied by a large $\sim 6\%$ lattice strain, which makes it unlikely that practical thermoelectric modules could be made based on this material. Furthermore, heavy n-type doping of PbTiO_3 may be particularly challenging because of the presence of Pb^{2+} , which might lead to low energy compensating defects associated with availability of the Pb^{4+} valence state.

The results suggest that in addition to SrTiO_3 ,

KNbO_3 , and perhaps its alloys such as $(\text{K},\text{Na})\text{NbO}_3$ may be particularly good candidate materials. We also find that rutile TiO_2 is a good candidate and is remarkable in that it is a binary, non-perovskite based compound.

The key challenge in developing any of these oxides into high performance thermoelectrics will be doping. As mentioned, in SrTiO_3 and TiO_2 doping can be done by Nb alloying on the Ti site. However, the CBM’s have Ti d character, which means that other doping strategies should be explored. Both YTiO_3 and LaTiO_3 form in perovskite structure and so exploration of the solid solutions with SrTiO_3 would be one avenue. Another would be doping on the O site, perhaps with F.

In the case of TiO_2 , the possibilities other than Nb doping are more limited, but again it may be possible to use the O site. This is consistent with transport measurements on titania doped by oxygen deficiency. [54] TiOF can be formed in a tetragonal rutile structure, [55] suggesting that there could be a high solubility of F in rutile TiO_2 . One issue with TiO_2 is the tendency of the binary oxide to oxygen deficiency when processed at high temperature under reducing conditions. This O deficiency, if large, can lead to ordered phases, $\text{Ti}_n\text{O}_{2n-1}$, known as Magneli phases. [56–58] These conducting phases are generally made by reduction of TiO_2 at temperatures above 1300 K. [58] While these phases have several desirable properties for thermoelectrics, so far the thermopowers obtained are too low to obtain high ZT . [54, 59–61] It would be important to avoid the formation of Magneli phases in assessing doped rutile TiO_2 as a thermoelectric. F doping and avoidance of high temperature anneals in reducing environments may be useful for this. Doping of KNbO_3 , or $(\text{K},\text{Na})\text{NbO}_3$ is also expected to be a challenge, although the required doping level is lower than for the other compounds studied. Some possibilities could be divalent substitutions on the K site, such as Ba or again F on the O site. In this regard, it is known that BaNbO_3 forms in a perovskite structure and is metallic. [62]

In summary, we present simple screens that can be readily applied in searching for new oxide thermoelectrics and demonstrate them by application to a set of oxides. This includes a simple screen based on energy isosurface structure. This provides a visual search strategy. We find that KNbO_3 and rutile TiO_2 are interesting compounds to investigate further as potential thermoelectrics in addition to the known thermoelectric compound SrTiO_3 .

Work at the University of Missouri (JS, DJS) is supported by the U.S. Department of Energy, Basic Energy Sciences through the S3TEC Energy Frontier Research Center, award de-sc0001299/DE-FG02-09ER46577. KPO is grateful for support from the Institute of High Performance Computing (IHPC) A*STAR.

[1] C. Wood, Rep. Prog. Phys. **51**, 459 (1988).

[2] S. B. Riffat and X. L. Ma, Appl. Thermal Eng. **23**, 913 (2003).

[3] J. Yang and T. Caillat, MRS Bull. **31**, 224 (2006).

[4] F. J. DiSalvo, Science **285**, 703 (1999).

[5] D. Kraemer, B. Poudel, H. Feng, C. Caylor, B. Yu,

- X. Yan, Y. Ma, X. Wang, D. Wang, A. Muto, M. McEneaney, M. Chiesa, Z. Ren, and G. Chen, *Nature Materials* **10**, 532 (2011).
- [6] K. Kumar, S. D. Heister, X. Xu, J. R. Salvador, and G. P. Meisner, *J. Electron. Mater.* **42**, 665 (2013).
- [7] L. D. Hicks and M. S. Dresselhaus, *Phys. Rev. B* **47**, 12727 (1993).
- [8] K. Kuroki and R. Arita, *J. Phys. Soc. Jpn.* **76**, 083707 (2007).
- [9] X. Chen, D. Parker, and D. J. Singh, *Sci. Rep.* **3**, 3168 (2013).
- [10] H. Usui, K. Suzuki, K. Kuroki, S. Nakano, K. Kudo, and M. Nohara, *Phys. Rev. B* **88**, 075140 (2013).
- [11] H. Usui, S. Shibata, and K. Kuroki, *Phys. Rev. B* **81**, 205121 (2010).
- [12] K. Shirai and K. Yamanaka, *J. Appl. Phys.* **113**, 053705 (2013).
- [13] D. Parker, X. Chen, and D. J. Singh, *Phys. Rev. Lett.* **110**, 146601 (2013).
- [14] N. A. Mecholsky, L. Resca, I. L. Pegg, and M. Fornari, *Phys. Rev. B* **89**, 155131 (2014).
- [15] Y. Pei, X. Shi, A. LaLonde, H. Wang, L. Chen, and G. J. Snyder, *Nature (London)* **473**, 66 (2011).
- [16] L. Bjerg, G. K. H. Madsen, and B. B. Iversen, *Chem. Mater.* **23**, 3907 (2011).
- [17] I. Ohkubo and T. Mori, *Chem. Mater.* **27**, 7265 (2015).
- [18] H. Shi, D. Parker, M. H. Du, and D. J. Singh, *Phys. Rev. Appl.* **3**, 014004 (2015).
- [19] G. K. H. Madsen, *J. Am. Chem. Soc.* **128**, 12140 (2006).
- [20] S. Curtarolo, G. L. W. Hart, M. B. Nardelli, N. Mingo, S. Sanvito, and O. Levy, *Nature Materials* **12**, 191 (2013).
- [21] S. D. Wang, Z. Wang, W. Setyawan, N. Mingo, and S. Curtarolo, *Phys. Rev. X* **1**, 021012 (2011).
- [22] S. Bhattacharaya and G. K. H. Madsen, *Phys. Rev. B* **92**, 085205 (2015).
- [23] J. W. Fergus, *J. Eur. Ceram. Soc.* **32**, 525 (2012).
- [24] K. Koumoto, Y. Wang, R. Zhang, A. Kosuga, and R. Funahashi, *Ann. Rev. Mater. Res.* **40**, 363 (2010).
- [25] I. Terasaki, Y. Sasago, and K. Uchinokura, *Phys. Rev. B* **56**, R12685 (1997).
- [26] S. Hebert, S. Lambert, D. Pelloquin, and A. Maignan, *Phys. Rev. B* **64**, 172101 (2001).
- [27] Y. Miyazaki, M. Onoda, T. Oku, K. Kikuchi, Y. Ishii, Y. Ono, Y. Morii, and T. Kajitana, *J. Phys. Soc. Jpn.* **71**, 491 (2002).
- [28] K. Koumoto, I. Terasaki, and R. Funahashi, *MRS Bull.* **31**, 206 (2006).
- [29] M. Ohtaki, K. Araki, and K. Yamamoto, *J. Electr. Mater.* **38**, 1234 (2009).
- [30] P. Jood, R. J. Mehta, Y. Zhang, T. Borca-Tasciuc, S. X. Dou, D. J. Singh, and G. Ramanath, *RSC Adv.* **4**, 6363 (2014).
- [31] K. P. Ong, D. J. Singh, and P. Wu, *Phys. Rev. B* **83**, 115110 (2011).
- [32] D. J. Singh and L. Nordstrom, *Planewaves Pseudopotentials and the LAPW Method, 2nd Edition* (Springer, Berlin, 2006).
- [33] P. Blaha, K. Schwarz, G. Madsen, D. Kvasnicka, and J. Luitz, WIEN2k, An Augmented Plane Wave + Local Orbitals Program for Calculating Crystal Properties (K. Schwarz, Tech. Univ. Wien, Austria) (2001).
- [34] J. P. Perdew, K. Burke, and M. Ernzerhof, *Phys. Rev. Lett.* **77**, 3865 (1996).
- [35] F. Tran and P. Blaha, *Phys. Rev. Lett.* **102**, 226401 (2009).
- [36] D. Koller, F. Tran, and P. Blaha, *Phys. Rev. B* **83**, 195134 (2011).
- [37] D. J. Singh, *Phys. Rev. B* **82**, 155145 (2010).
- [38] Y. S. Kim, M. Marsman, G. Kresse, F. Tran, and P. Blaha, *Phys. Rev. B* **82**, 205212 (2010).
- [39] D. J. Singh, *Phys. Rev. B* **82**, 205102 (2010).
- [40] G. K. H. Madsen and D. J. Singh, *Comput. Phys. Commun.* **175**, 67 (2006).
- [41] J. Kolodziejczak and S. Zukotynski, *Phys. Status Solidi (b)* **5**, 145 (1964).
- [42] D. S. Parker, A. F. May, and D. J. Singh, *Phys. Rev. Appl.* **3**, 064003 (2015).
- [43] E. A. Wood, *Acta Cryst.* **4**, 353 (1951).
- [44] K. E. Johnston, C. C. Tang, J. E. Parker, K. S. Knight, P. Lightfoot, and S. E. Ashbrook, *J. Am. Chem. Soc.* **132**, 8732 (2010).
- [45] D. J. Singh and I. I. Mazin, *Phys. Rev. B* **56**, R1650 (1997).
- [46] A. F. May, D. J. Singh, and G. J. Snyder, *Phys. Rev. B* **79**, 153101 (2009).
- [47] D. J. Singh, *Phys. Rev. B* **81**, 195217 (2010).
- [48] X. Fan, W. Zheng, X. Chen, and D. J. Singh, *Plos One* **9**, e91423 (2014).
- [49] D. Bayerl and E. Kioupakis, *Phys. Rev. B* **91**, 165104 (2015).
- [50] S. Ohta, T. Nomura, H. Ohta, M. Hirano, H. Hosono, and K. Koumoto, *Appl. Phys. Lett.* **87**, 092108 (2005).
- [51] N. Wang, H. Chen, H. He, W. Norimatsu, M. Kusunoki, and K. Koumoto, *Sci. Rep.* **3**, 3449 (2013).
- [52] M. Tachibana, T. Kolodiazny, and E. Takayama-Moromachi, *Appl. Phys. Lett.* **93**, 092902 (2008).
- [53] W. R. Thurber and A. J. H. Mante, *Phys. Rev.* **139**, A1655 (1965).
- [54] M. Backhaus-Ricoult, J. R. Rustad, L. Moore, C. Smith, and J. Brown, *Appl. Phys. A* **116**, 433 (2014).
- [55] B. L. Chamberland and A. W. Sleight, *Solid State Commun.* **5**, 765 (1967).
- [56] S. Andersson and A. Magneli, *Die Naturwissenschaften* **43**, 495 (1956).
- [57] S. Andersson, B. Collen, U. Kylenstierna, and A. Magneli, *Acta Chem. Scand.* **11**, 1641 (1957).
- [58] F. C. Walsh and R. G. A. Wills, *Electrochimica Acta* **55**, 6342 (2010).
- [59] S. Harada, K. Tanaka, and H. Inui, *J. Appl. Phys.* **108**, 083703 (2010).
- [60] D. Portehault, V. Maneeratana, C. Candolfi, N. Oeschler, I. Veremchuk, Y. Grin, C. Sanchez, and M. Antonietti, *ACS Nano* **5**, 9052 (2011).
- [61] M. Backhaus-Ricoult, J. R. Rustad, D. Vargheese, I. Dutta, and K. Work, *J. Electronic Materials* **41**, 1636 (2012).
- [62] M. T. Casais, J. A. Alonso, I. Rasines, and M. A. Hidalgo, *MRS Bull.* **30**, 201 (1995).

FIGURE CAPTIONS

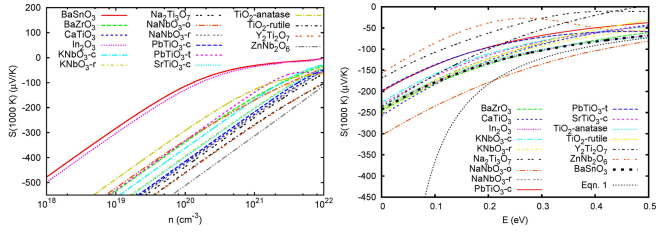


FIG. 1. $S(1000\text{ K})$ as a function of doping level on a log scale (left) and as function of Fermi energy, E_F (right). For non-cubic materials the thermopower shown is the ceramic average, $S_{av} = (\sigma_{xx}S_{xx} + \sigma_{yy}S_{yy} + \sigma_{zz}S_{zz})/(\sigma_{xx} + \sigma_{yy} + \sigma_{zz})$. In the right panel the limiting formula, Eqn. 1 is also plotted, and a heavier dashed line is shown for BaSnO₃, which has a single almost perfectly isotropic parabolic band at the CBM, illustrating the behavior of a SPB.

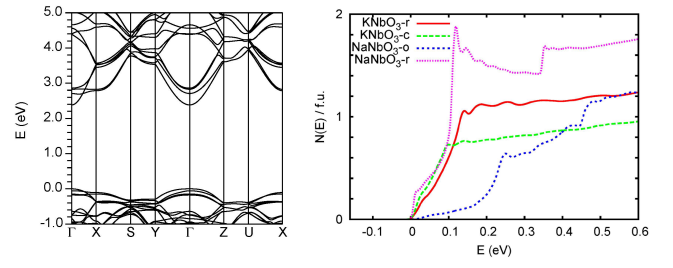


FIG. 2. Band structure (left) of orthorhombic NaNbO₃ and DOS (right) for different structures of NaNbO₃ and KNbO₃ on a per formula unit base, with the energy zero set to the CBM.

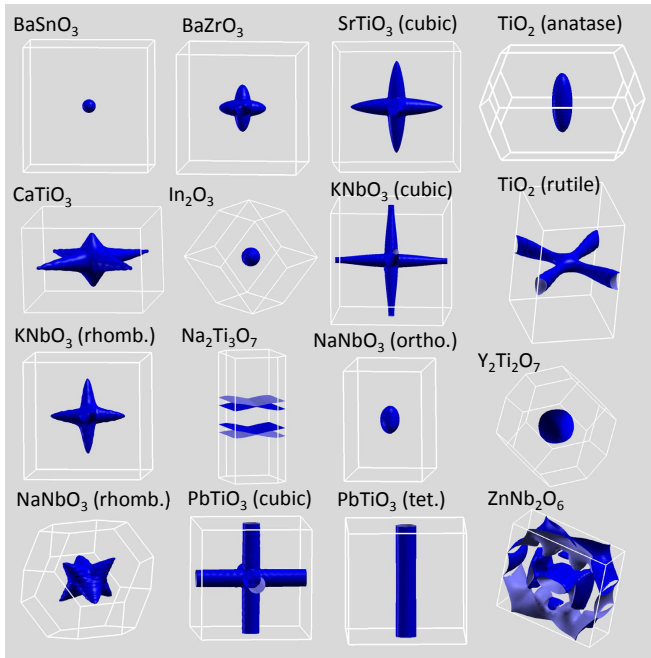


FIG. 3. Isoenergy surfaces 100 meV above the conduction band minimum for candidate oxide materials. Several of the compounds also have smaller isosurface sheets enclosed inside the sheet shown (see text).

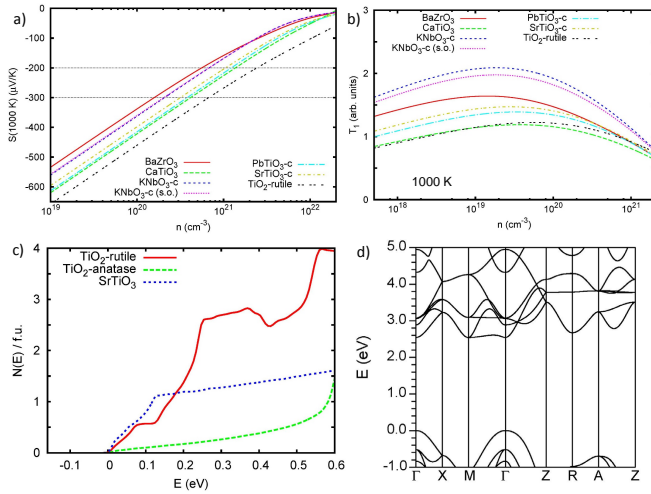


FIG. 4. (a) Doping dependent thermopower at 1000 K for the best identified materials, (b) transport function T_1 (see text), (c) DOS for TiO_2 and cubic SrTiO_3 , (d) band structure of rutile TiO_2 .